An Evaluation of River Bank Erosion in Volcanic Rivers Post Eruption 2010 of Mount Merapi

Puji HARSANTO[1], Jazaul IKHSAN[1], and Hiroshi TAKEBAYASHI[2]

[1] Dept. of Civil Engineering, Muhammadiyah University of Yogyakarta (Jl. Ring Road Selatan, Kasihan, Bantul, Indonesia)
E-mail: puji_hr@yahoo.com

[2] Disaster Prevent Research Institute, Kyoto University (Gokasyo, Uji, Kyoto 6110011, Japan)

Mt. Merapi is one of the most active volcanoes in Indonesia. Its eruptions have caused disasters in downstream areas. Some of rivers that the origin located at Mt. Merapi have a large amount of sediment resources, after eruption on October-November 2010. The total volume of sediment released during eruption is estimated at 150 million m^3. Sediment was deposited at the upstream area of the rivers. When the rainfall which has a high intensity occurs, the deposited sediment will flows to the downstream area as bed-load transport. Furthermore, the phenomenon of flow with high concentration occurs in the rivers. Using numerical simulation, the impact of high concentration of bed-load transport is applied in Progo River, Yogyakarta, Indonesia. The results show that the high bed-load transport rate increase the bar grow rate. Its increase the bed degradation near the bank toe and then the bank collapse possibility is increase also. Furthermore, the bank erosion problem after 2010 Mt. Merapi eruption should be considered intensively.

Key words: volcanic rivers, bed-load transport rate, river bed morphology, bank erosion potential

1. INTRODUCTION

1.1 Background

In October 2010, Mt. Merapi in Central Java, Indonesia had a major eruption, which released approximately 130 million m^3 of lahar. The sediment was deposited at the upstream area and become a large amount of sediment resources of the downstream area. During rainy season the deposited lahar will transport to the downstream as bed-load transport. The volume of sediment transport in the flow is increase in this season. Its cause the exchanged of bed morphology of the river rapidly. The bed-load will be deposited at the low velocity regime (inner bend) and produce bar formation. The bar formation will reduce the flow area and tend to increase the flow velocity at the outer bend. The large of sediment resources in the river also have possibilities to increase the percentage of the volume of bed-load transport. In the other word, the volume of bed-load transport is higher than equilibrium condition.

The bank erosion is one of the processes of river morphology. General processes in bank erosions are explained in analytical concept by [*Osman and Thorne,* 1988] and *Thorne and Osman,* 1988]. In this concept, the processes of bank failure are mainly triggered by bed degradation near the bank. The bed degradation causes the increasing of the relative bank height and the potential for destabilization of the bank with respect to mass failure will decrease. So, the bed degradation is the important factor on triggering bank erosion. Recently, many researchers also use bed degradation near the bank toe as the main factor on triggering bank failure [*Duan and Julien,* 2005]. The failure concept from those researchers indicates that the analysis of bed degradation near the bank toe is one of the important for analysis on bank erosion problem. Hence, in this study, field investigations were conducted to obtain the morphology characteristics of riverbed due to the bed-load transport rate. Furthermore, the bed degradations analysis near the bank toe is observed.

1.2 Study area

The river reach of Progo River in Bantar is chosen in order to examine the interaction of

channel geometry, concentration of be-load and bed deformation. The watershed area of Progo River is around 17,432 square kilometers. The headwaters are located in the Mt. Merapi. Due to the major eruption in October 2010, the amount of sediment resources at the tributary of Progo River (Putih River for example), were increased significantly. **Fig. 1** shows the Progo River system. The figure shows that Putih River, Blongkeng River and Pabelan River are the tributaries of Progo River. Post 2010 Mt. Merapi's eruption, 5.36 million m^3 material was deposited in Putih River as shown in **Fig. 2**. The material is in unstable condition. During rainy season, the material moves to the downstream as debris flow causes the concentration of bed-load transport is higher than the equilibrium condition.

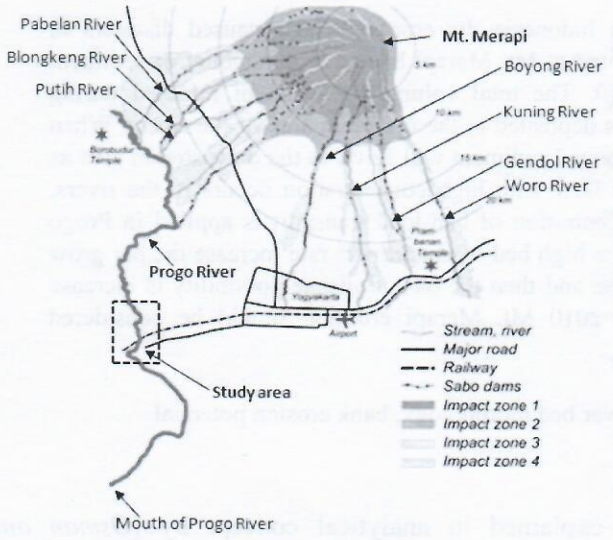

Figure 1. Progo River System and location fo study area

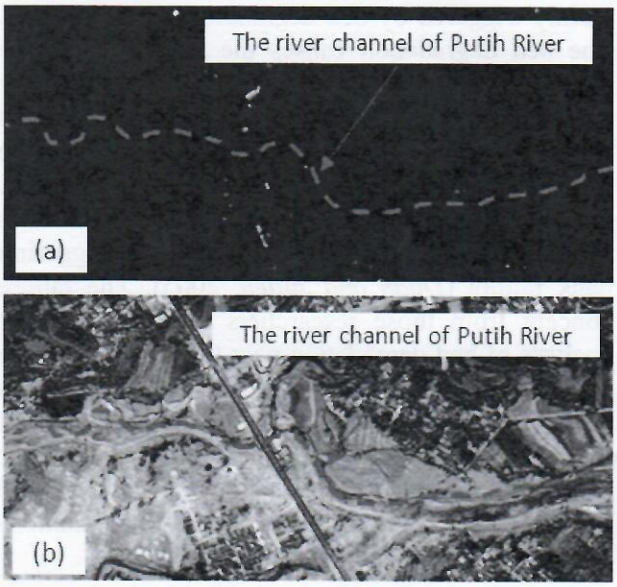

Figure 2. The sediment resources in Putih River before and after 2010 Mt. Merapi eruption

2. NUMERICAL MODEL

Numerical simulations are performed using the horizontal two-dimensional flow model which the equations are written in general coordinate system. The model uses the finite difference method to solve the different equations. Relationship between Cartesian coordinate system and General coordinate system is as follows.

$$J = \frac{1}{\left(\frac{\partial x}{\partial \xi}\frac{\partial y}{\partial \eta} - \frac{\partial x}{\partial \eta}\frac{\partial y}{\partial \xi}\right)} \tag{1a}$$

$$\frac{\partial \xi}{\partial x} = J\frac{\partial y}{\partial \eta} \tag{1b}$$

$$\frac{\partial \eta}{\partial x} = -J\frac{\partial y}{\partial \xi} \tag{1c}$$

$$\frac{\partial \xi}{\partial y} = -J\frac{\partial x}{\partial \eta} \tag{1d}$$

$$\frac{\partial \eta}{\partial y} = J\frac{\partial x}{\partial \xi} \tag{1e}$$

Where, ξ and η are the coordinates along the longitudinal and the transverse directions in generalized coordinate system, respectively, x and y are the coordinates in Cartesian coordinate system. Computation of surface flow is carried out using the governing equation of the horizontal two-dimensional flow averaged with depth. The conservation of mass, i.e., inflow and outflow of mass by seepage flow, is taken into consideration as shown in the following equation [*Takebayashi,* 2005].

$$\Lambda\frac{\partial}{\partial t}\left(\frac{z}{J}\right)+\frac{\partial}{\partial \xi}\left(\left(\frac{\partial \xi}{\partial t}+U\right)\frac{h}{J}\right)+\frac{\partial}{\partial \eta}\left(\left(\frac{\partial \eta}{\partial t}+V\right)\frac{h}{J}\right)+\frac{\partial}{\partial \xi}\left(\left(\frac{\partial \xi}{\partial t}+U_g\right)\frac{h_g}{J}\right)+\frac{\partial}{\partial \eta}\left(\left(\frac{\partial \eta}{\partial t}+V_g\right)\frac{h_g}{J}\right)=0 \tag{2}$$

Where, t is the time, z is the water surface level. Surface flow depth is represented as h, seepage flow depth is h_g. U and V represent the contra variant depth averaged flow velocity on bed along ξ and η coordinates, respectively.

These velocities are defined as

$$U = \frac{\partial \xi}{\partial x}u + \frac{\partial \xi}{\partial y}v \tag{3a}$$

$$V = \frac{\partial \eta}{\partial x}u + \frac{\partial \eta}{\partial y}v \tag{3b}$$

where, u and v represent depth averaged flow velocity on bed along x and y coordinates, respectively. U_g and V_g represent the contra variant depth averaged seepage flow velocity along ξ and η coordinates, respectively. These velocities are defined as

$$U_g = \frac{\partial \xi}{\partial x} u_g + \frac{\partial \xi}{\partial y} v_g \tag{4a}$$

$$V_g = \frac{\partial \eta}{\partial x} u_g + \frac{\partial \eta}{\partial y} v_g \tag{4b}$$

where, depth averaged seepage flow velocities along x and y coordinates in Cartesian coordinate *system* are shown as u_g, v_g, respectively. Λ is a parameter related to the porosity in the soil, wherein $\Lambda = 1$ as z γ z_b, and $\Lambda = \lambda$ as $z < z_b$, where z_b is the bed level and λ is the porosity in the soil. Seepage flow is assumed as horizontal two-dimensional saturation flow. Momentum equations of surface water are as follows.

$$\begin{aligned}
&\frac{\partial}{\partial t}\left(\frac{hU}{J}\right)+\frac{\partial}{\partial \xi}\left(\left(\frac{\partial \xi}{\partial t}+U\right)\frac{hU}{J}\right)+\frac{\partial}{\partial \eta}\left(\left(\frac{\partial \eta}{\partial t}+V\right)\frac{hU}{J}\right)\\
&-\frac{hu}{J}\left(\frac{\partial}{\partial t}\left(\frac{\partial \xi}{\partial x}\right)+\left(\frac{\partial \xi}{\partial t}+U\right)\frac{\partial}{\partial \xi}\left(\frac{\partial \xi}{\partial x}\right)+\left(\frac{\partial \eta}{\partial t}+V\right)\frac{\partial}{\partial \eta}\left(\frac{\partial \xi}{\partial x}\right)\right)\\
&-\frac{hv}{J}\left(\frac{\partial}{\partial t}\left(\frac{\partial \xi}{\partial y}\right)+\left(\frac{\partial \xi}{\partial t}+U\right)\frac{\partial}{\partial \xi}\left(\frac{\partial \xi}{\partial y}\right)+\left(\frac{\partial \eta}{\partial t}+V\right)\frac{\partial}{\partial \eta}\left(\frac{\partial \xi}{\partial y}\right)\right)\\
&=-gh\left(\frac{1}{J}\left(\left(\frac{\partial \xi}{\partial x}\right)^2+\left(\frac{\partial \xi}{\partial y}\right)^2\right)\frac{\partial z_s}{\partial \xi}+\frac{1}{J}\left(\frac{\partial \xi}{\partial x}\frac{\partial \eta}{\partial x}+\frac{\partial \xi}{\partial y}\frac{\partial \eta}{\partial y}\right)\frac{\partial z_s}{\partial \eta}\right)-\frac{\tau_{bs}}{\rho J}\\
&+\frac{1}{J}\left(\frac{\partial \xi}{\partial x}\right)^2\frac{\partial}{\partial \xi}(h\sigma_{xx})+\frac{1}{J}\frac{\partial \xi}{\partial x}\frac{\partial \eta}{\partial x}\frac{\partial}{\partial \eta}(h\sigma_{xx})+\frac{1}{J}\frac{\partial \xi}{\partial x}\frac{\partial \eta}{\partial x}\frac{\partial}{\partial \eta}(h\tau_{xy})+\frac{1}{J}\frac{\partial \xi}{\partial y}\frac{\partial \xi}{\partial x}\frac{\partial}{\partial \xi}(h\tau_{xy})\\
&+\frac{1}{J}\frac{\partial \xi}{\partial x}\frac{\partial \eta}{\partial y}\frac{\partial}{\partial \eta}(h\tau_{xy})+\frac{1}{J}\frac{\partial \xi}{\partial x}\frac{\partial \xi}{\partial y}\frac{\partial}{\partial \xi}(h\tau_{xy})+\frac{1}{J}\left(\frac{\partial \xi}{\partial y}\right)^2\frac{\partial}{\partial \xi}(h\sigma_{yy})+\frac{1}{J}\frac{\partial \xi}{\partial y}\frac{\partial \eta}{\partial y}\frac{\partial}{\partial \eta}(h\sigma_{yy})
\end{aligned} \tag{5a}$$

$$\begin{aligned}
&\frac{\partial}{\partial t}\left(\frac{hV}{J}\right)+\frac{\partial}{\partial \xi}\left(\left(\frac{\partial \xi}{\partial t}+U\right)\frac{hV}{J}\right)+\frac{\partial}{\partial \eta}\left(\left(\frac{\partial \eta}{\partial t}+V\right)\frac{hV}{J}\right)\\
&-\frac{hu}{J}\left(\frac{\partial}{\partial t}\left(\frac{\partial \eta}{\partial x}\right)+\left(\frac{\partial \xi}{\partial t}+U\right)\frac{\partial}{\partial \xi}\left(\frac{\partial \eta}{\partial x}\right)+\left(\frac{\partial \eta}{\partial t}+V\right)\frac{\partial}{\partial \eta}\left(\frac{\partial \eta}{\partial x}\right)\right)\\
&-\frac{hv}{J}\left(\frac{\partial}{\partial t}\left(\frac{\partial \eta}{\partial y}\right)+\left(\frac{\partial \xi}{\partial t}+U\right)\frac{\partial}{\partial \xi}\left(\frac{\partial \eta}{\partial y}\right)+\left(\frac{\partial \eta}{\partial t}+V\right)\frac{\partial}{\partial \eta}\left(\frac{\partial \eta}{\partial y}\right)\right)\\
&=-gh\left(\frac{1}{J}\left(\frac{\partial \xi}{\partial x}\frac{\partial \eta}{\partial x}+\frac{\partial \xi}{\partial y}\frac{\partial \eta}{\partial y}\right)\frac{\partial z_s}{\partial \xi}+\frac{1}{J}\left(\left(\frac{\partial \eta}{\partial x}\right)^2+\left(\frac{\partial \eta}{\partial y}\right)^2\right)\frac{\partial z_s}{\partial \eta}\right)-\frac{\tau_{bs}}{\rho J}\\
&+\frac{1}{J}\frac{\partial \eta}{\partial x}\frac{\partial \xi}{\partial x}\frac{\partial}{\partial \xi}(h\sigma_{xx})+\frac{1}{J}\left(\frac{\partial \eta}{\partial x}\right)^2\frac{\partial}{\partial \eta}(h\sigma_{xx})+\frac{1}{J}\frac{\partial \eta}{\partial y}\frac{\partial \xi}{\partial x}\frac{\partial}{\partial \xi}(h\tau_{xy})+\frac{1}{J}\frac{\partial \eta}{\partial y}\frac{\partial \eta}{\partial x}\frac{\partial}{\partial \eta}(h\tau_{xy})\\
&+\frac{1}{J}\frac{\partial \eta}{\partial x}\frac{\partial \xi}{\partial y}\frac{\partial}{\partial \xi}(h\tau_{xy})+\frac{1}{J}\frac{\partial \eta}{\partial x}\frac{\partial \eta}{\partial y}\frac{\partial}{\partial \eta}(h\tau_{xy})+\frac{1}{J}\frac{\partial \eta}{\partial y}\frac{\partial \xi}{\partial y}\frac{\partial}{\partial \xi}(h\sigma_{yy})+\frac{1}{J}\left(\frac{\partial \eta}{\partial y}\right)^2\frac{\partial}{\partial \eta}(h\sigma_{yy})
\end{aligned} \tag{5b}$$

Where, g is the gravity, ρ is the water density. $\tau_{b\xi}$ and $\tau_{b\eta}$ represent the contra variant shear stress along ξ and η coordinates, respectively. These shear stresses are defined as

$$\tau_{b\xi} = \frac{\partial \xi}{\partial x}\tau_{bx} + \frac{\partial \xi}{\partial y}\tau_{by} \tag{6a}$$

$$\tau_{b\eta} = \frac{\partial \eta}{\partial x}\tau_{bx} + \frac{\partial \eta}{\partial y}\tau_{by} \tag{6b}$$

where, τ_x and τ_y are the shear stress along x and y coordinates, respectively as follows.

$$\tau_x = \tau_b \frac{u_b}{\sqrt{u_b^2 + v_b^2}} \tag{7a}$$

$$\tau_y = \tau_b \frac{v_b}{\sqrt{u_b^2 + v_b^2}} \tag{7b}$$

$$\frac{\tau_b}{\rho} = u_*^2 \tag{8}$$

$$u_*^2 = \frac{n_m^2 g}{R^{1/3}}\left(u^2 + v^2\right) \tag{9}$$

Where, u_* is the friction velocity, n_m is the Manning's roughness coefficient, R is the hydraulic radius, k_s is the roughness height. u_b and v_b represent velocity near the bed surface along x and y coordinates, respectively. Velocities near the bed are evaluated using curvature radius of streamlines as follows.

$$u_b = u_{bs}\cos\alpha_s - v_{bs}\sin\alpha_s \tag{10a}$$

$$v_b = u_{bs}\sin\alpha_s + v_{bs}\cos\alpha_s \tag{10b}$$

$$u_{bs} = 8.5u_* \tag{11}$$

$$v_{bs} = -N_* \frac{h}{r} u_{bs} \tag{12}$$

Where, $\alpha_s = \arctan(v/u)$, N_* is 7.0 [*Engelund,* 1974] and r is the curvature radius of stream lines obtained by depth integrated velocity field as follows [*Shimizu and Itakura*, 1991].

$$\frac{1}{r} = \frac{1}{\left(u^2+v^2\right)^{3/2}}\left\{u\left(u\frac{\partial v}{\partial x} - v\frac{\partial u}{\partial x}\right) + v\left(u\frac{\partial v}{\partial y} - v\frac{\partial u}{\partial y}\right)\right\} \tag{13}$$

σ_{xx}, σ_{yy}, τ_{xy} and τ_{yx} are turbulence stresses as follows.

$$\sigma_{xx} = 2\nu\frac{\partial u}{\partial x} \tag{14a}$$

$$\sigma_{yy} = 2\nu\frac{\partial v}{\partial y} \tag{14b}$$

$$\tau_{xy} = \tau_{yx} = \nu\left(\frac{\partial v}{\partial x} + \frac{\partial u}{\partial y}\right) \tag{15}$$

$$\nu = \frac{\kappa}{6}u_* h \tag{16}$$

Where, ν is the coefficient of kinematics eddy viscosity, κ is the Karman constant, k_t is the depth-averaged turbulence kinetic energy [*Takebayashi,* 2005].

$$u_g = -k_{gx}\left(\frac{\partial \xi}{\partial x}\frac{\partial z_b}{\partial \xi} + \frac{\partial \eta}{\partial x}\frac{\partial z_b}{\partial \eta}\right) \tag{17a}$$

$$v_g = -k_{gy}\left(\frac{\partial \xi}{\partial y}\frac{\partial z_b}{\partial \xi}+\frac{\partial \eta}{\partial y}\frac{\partial z_b}{\partial \eta}\right) \tag{17b}$$

Where, k_{gx} and k_{gy} is the coefficient of permeability along the longitudinal and the transverse directions, respectively. When the water depth of surface flow becomes less than the mean diameter of the bed material, the surface flow is computed only in consideration of the pressure term and bed shear stress term in the momentum equation of surface flow [*Nagata,* 1999].

Grain size distribution is evaluated using the sediment transport multilayer model as follows [*Takebayashi, et al,.* 2003]:

$$\frac{\partial}{\partial t}\left(\frac{c_b E_b f_{bk}}{J}\right)+(1-\lambda)F_{bk}\frac{\partial}{\partial t}\left(\frac{z_b}{J}\right) + \left(\frac{\partial}{\partial \xi}\left(\frac{\partial \xi}{\partial t}\frac{c_b E_b f_{bk} r_b}{J}+\frac{q_{b\xi k}}{J}\right)+\frac{\partial}{\partial \eta}\left(\frac{\partial \eta}{\partial t}\frac{c_b E_b f_{bk} r_b}{J}+\frac{q_{b\eta k}}{J}\right)\right)=0 \tag{18a}$$

$$\begin{cases} F_{bk} = f_{d1k}, \ \partial z_b/\partial t \le 0 \\ F_{bk} = f_{bk}, \ \partial z_b/\partial t \ge 0 \end{cases} \tag{18b}$$

$$\frac{\partial}{\partial t}\left(\frac{E_{d1} f_{d1k}}{J}\right)-F_{dk}\frac{\partial}{\partial t}\left(\frac{E_{d1}}{J}\right)=0 \qquad \begin{cases} F_{dk} = f_{d1k}, \ \partial z_b/\partial t \le 0 \\ F_{dk} = f_{bk}, \ \partial z_b/\partial t \ge 0 \end{cases} \tag{18c}$$

In the formulae above, f_{bk} is the concentration of bed-load of size class k in the bed-load layer, f_{dlk} is the sediment concentration of size class k in the m^{th} bed layer, c_b is the depth-averaged concentration of bed-load. E_{be} is the equilibrium bed-load layer thickness; it is estimated by the following equation [*Egashira and Ashida,* 1992]:

$$\frac{E_{be}}{d_m} = \frac{1}{c_b \cos\theta\left(\tan\phi - \tan\theta\right)}\tau_{*m} \tag{19}$$

where d_m is the mean diameter of bed-load, ϕ is the angle of repose, and τ_{*m} is the non-dimensional shear stress of mean diameter. E_{sd} is the sediment layer thickness on cohesive sediment bed. E_b is the bed-load layer thickness, $q_{b\xi k}$ and $q_{b\eta k}$ are the bed-load of size class k in ξ and η directions, respectively, q_{bxk} and q_{byk} are the bed-load of size class k in x and y directions, respectively as follows [*Ashida and Michiue*, 1972; *Kovacs and Parker*, 1994 and *Liu*, 1991].

$$q_{bxk} = q_{bk}\cos\beta_k \tag{20a}$$

$$q_{byk} = q_{bk}\sin\beta_k \tag{20b}$$

$$q_{bk} = 17\frac{\rho u_{*e}^3}{(\rho_s-\rho)g}\left(1-\sqrt{K_c}\frac{u_{*ck}}{u_*}\right)\left(1-K_c\frac{u_{*ck}^2}{u_*^2}\right)f_{bk} \tag{20c}$$

Therein, ρ_s is the sediment density, u_{*e} is the effective shear velocity, the non-dimensional critical friction velocity of size class k is evaluated as follows [*Ashida and Michiue*, 1972].

$$u_{*ck}^2 = u_{*cm}^2\left[\frac{\log_{10}19}{\log_{10}(19\,d_k/d_m)}\right]^2\frac{d_k}{d_m} \tag{21a}$$

$$d_k/d_m \ge 0.4 \tag{21b}$$

$$u_{*ck}^2 = 0.85u_{*cm}^2 \tag{22a}$$

$$d_k/d_m \le 0.4 \tag{22b}$$

Iwagaki's formula [*Iwagaki*, 1956] which is formulated for uniform bed material is used for evaluating u_{*cm}. K_c is the correction factor due to the influence of bed inclination on sediment motion.

$$K_c = 1+\frac{1}{\mu_s}\left[\left(\frac{\rho}{\rho_s-\rho}+1\right)\cos\alpha\tan\theta_x+\sin\alpha\tan\theta_y\right] \tag{23}$$

where α is the angle of deviation of near-bed flow from the x direction as follows.

$$\alpha = \arctan\left(\frac{v_b}{u_b}\right) \tag{24}$$

μ_s is the coefficient of static friction. θ_x and θ_y are bed inclinations in x and y directions, respectively. These inclinations are evaluated as follows,

$$\theta_x = \arctan\left(\frac{\partial \xi}{\partial x}\frac{\partial z_b}{\partial \xi}+\frac{\partial \eta}{\partial x}\frac{\partial z_b}{\partial \eta}\right) \tag{25a}$$

$$\theta_y = \arctan\left(\frac{\partial \xi}{\partial y}\frac{\partial z_b}{\partial \xi}+\frac{\partial \eta}{\partial y}\frac{\partial z_b}{\partial \eta}\right) \tag{25b}$$

Hence, the local bed slope along direction of bed-load of sediment mean diameter (θ) is obtained as follows.

$$\sin\theta = \cos\beta_m\sin\theta_x+\sin\beta_m\sin\theta_y \tag{26}$$

where β_m is the deviation angle of bed-load of mean diameter to the x direction. The deviation angle of bed-load of size class k to the x direction (β_k), which depends on the flow near bed and inclination of the bed, is calculated by the following relation

$$\tan\beta_k = \frac{\sin\alpha-\Pi\Theta_y\left(\frac{u_{*ck}^2}{u_*^2}\right)\tan\theta_y}{\cos\alpha-\Pi\Theta_x\left(\frac{u_{*ck}^2}{u_*^2}\right)\tan\theta_x} \tag{27a}$$

$$\Pi = K_{ld}+1/\mu_s \tag{27b}$$

$$\Theta_y = \frac{1}{1+\tan^2\theta_x+\tan^2\theta_y} \tag{27c}$$

$$\Theta_x = \Theta_y + \frac{\rho}{\rho_s - \rho}\cos^2\theta_x \tag{27d}$$

Evolution of bed elevation is estimated by means of the following formulae

$$\frac{\partial}{\partial t}\left(\frac{c_b E_b}{J}\right)+(1-\lambda)\frac{\partial}{\partial t}\left(\frac{z_b}{J}\right)+\left(\frac{\partial}{\partial \xi}\left(\frac{\partial \xi}{\partial t}\frac{c_b E_b}{J}+\sum_{k=1}^{n}\frac{q_{bxk}}{J}\right)+\frac{\partial}{\partial \eta}\left(\frac{\partial \eta}{\partial t}\frac{c_b E_b}{J}+\sum_{k=1}^{n}\frac{q_{byk}}{J}\right)\right)=0 \tag{28}$$

In them, n represents the number of the size class of sediment.

3. SIMULATION SCENARIO

The river bed deformations were compared by applying two main conditions of bed-load transport rate at the upstream area. First condition is the bed-load transport at the upstream area same as the potential equilibrium sediment transport rate, q_b. The volume is 100% q_b namely Case1. The last condition is the bed-load transport more than q_b. These bed-load transport rates are 130% q_b and 150% q_b namely Case 2 and Case 3, respectively. It is describes the amount of sediment resources at the upstream area of the Progo River is large after 2010 eruption of Mt. Merapi.

To evaluate the bed deformation due to the bed-load transport rate condition, three cross sections, i.e. cross section 1-1, 2-2 and 3-3 are analyzed (see **Fig. 3**).

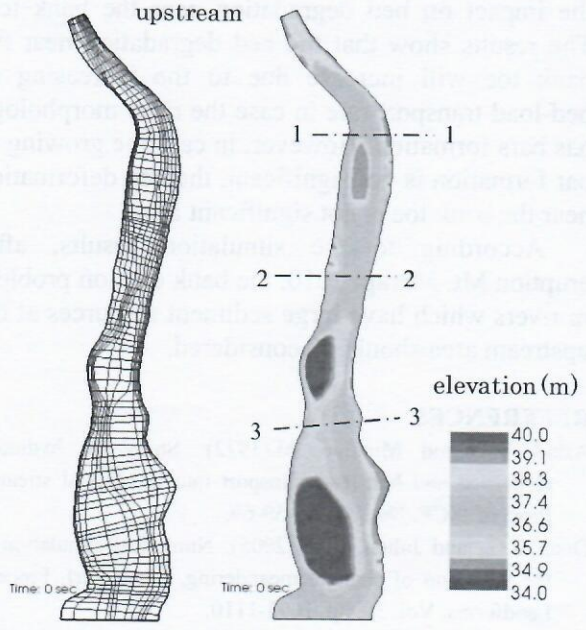

Figure 3. Grid and bed elevation in initial condition

4. RIVER BED MORPHOLOGY

In the opening of this paper, the evaluation of sediment transport volume on the potential of bank erosion was emphasized, and will be analyzed by the bed deformation on the bank toe. Indeed, bed-load transport may become an essential actor in tomorrow's sediment volume policies and all efforts must thus be focused on reducing their volume in the downstream area.

Fig. 4, **5**, and **6** are the bed deformation evolution at cross section 1-1 in Case 1, 2 and 3, respectively. In Case 1, the bed degradation near the bank toe at the right side was occurred (see **Fig. 4**). The bed degradation occurs more in Case 2 and Case 3 (see **Fig. 5** and **6**). The more bed-load transport in Case 2 and 3 produce the increasing of bar elevation in cross section 1-1. Furthermore, the flow velocities concentrated to the right bank side and produce more erosion on the riverbed. In cross section 2-2 and 3-3, the increasing of bar elevation is not so significant and the bed deformation at the bank toe is small as shown **Fig. 7** to **Fig. 12**. The results of numerical simulation indicate that the high concentration of bed-load transport rate not only produces the large sedimentation (the increasing of bar elevation), but also more erosion near the bank toe. Furthermore, the relative bank height will increase. This condition triggers the bank failure with planar mechanism [*Nagata*, 1999].

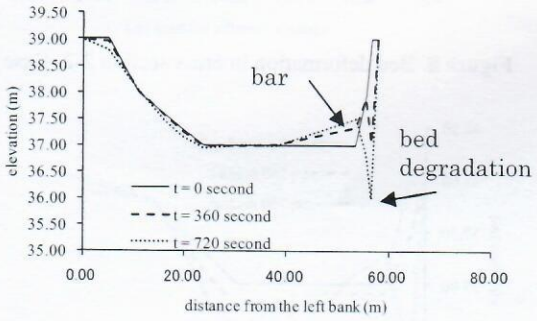

Figure 4. Bed deformation in cross section 1-1, Case 1

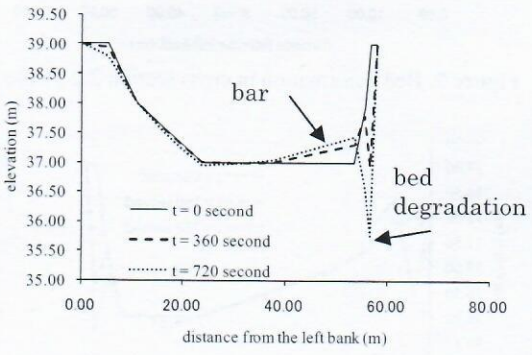

Figure 5. Bed deformation in cross section 1-1, Case 2

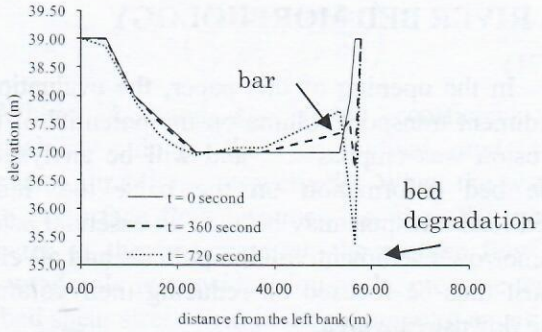

Figure 6. Bed deformation in cross section 1-1, Case 3

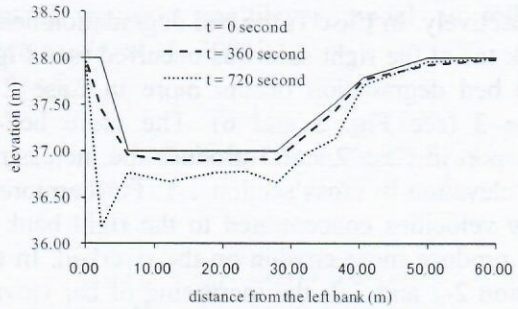

Figure 7. Bed deformation in cross section 2-2, Case 1

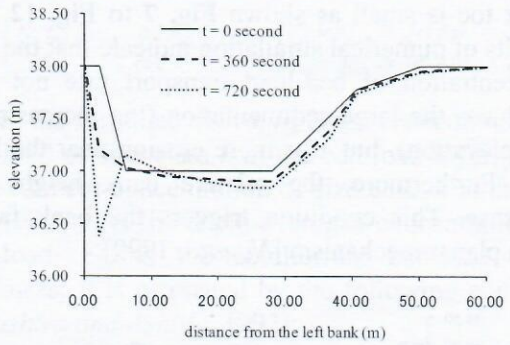

Figure 8. Bed deformation in cross section 2-2, Case 2

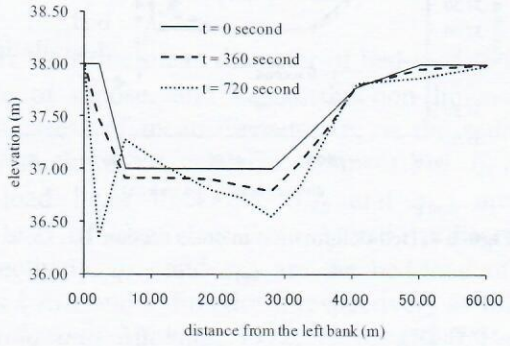

Figure 9. Bed deformation in cross section 2-2 , Case 3

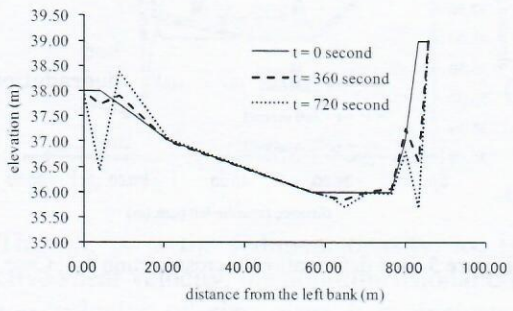

Figure 10. Bed deformation in cross section 3-3, Case 1

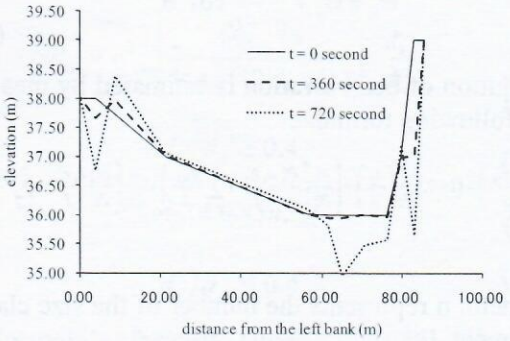

Figure 11. Bed deformation in cross section 3-3, Case 2

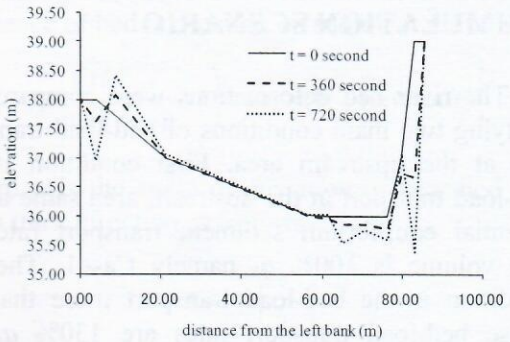

Figure 12. Bed deformation in cross section 3-3, Case 3

5. CONCLUSIONS

The horizontal two-dimensional bed deformation analysis of the Progo River at Bantar reach was performed. Two main methods of bed-load transport rates had been applied to evaluate the impact on bed degradation near the bank toe. The results show that the bed degradation near the bank toe will increase due to the increasing of bed-load transport rate in case the river morphology has bars formation. However, in case the growing of bar formation is not significant, the bed deformation near the bank toe is not significant also.

According to the simulation results, after eruption Mt. Merapi 2010, the bank erosion problem in rivers which have large sediment resources at the upstream area should be considered.

REFERENCES

Ashida, K. and Michiue, M.(1972): Study on hydraulic resistance and bed-load transport rate in alluvial streams, Proc. of JSCE, No. 206, pp.59-69.

Duan, J.G., and Julien, P.Y. (2005): Numerical simulation of the inception of channel meandering, Earth Surf. Process. Landforms, Vol. 30, pp. 1093-1110.

Egashira, S. and Ashida, K.(1992): Unified view of the mechanics of debris flow and bed-load, Advances in Micromechanics of Granular Materials, (Edited by H.H.Shen et al.) Elsevier, pp. 391-400.

Engelund, F. (1974): Flow and Bed Topography in Channel

Bends, Journal of Hydraulic Div., ASCE, Vol. 100, No. HY11.

Iwagaki, Y. (1956): Hydrodynamic study on critical shear stress. Proc. of JSCE, No. 41, pp. 1-21.

Kovacs, A. and Parker, G. (1994): A new vectorial bed-load formulation and its application to the time evolution of straight river channels. J. Fluid Mech. Vol. 267, pp. 153-183.

Liu, B.Y. (1991): Study on Sediment Transport and Bed Evolution in Compound Channels. Thesis presented to Kyoto University.

Nagata, N. (1999): Numerical Analysis of the 2-Dimensional Unsteady Flow Using a Generalized Coordinate System, The Lecture Collection on the Computer Use in Hydraulic Engineering, The Japan Society of Civil Engineers, pp. 51 – 76.

Osman, A.M., and Thorne, C.R. (1988): Riverbank stability analysis I: Theory, Journal of Hydraulic Engineering, Vol. 114, No. 2, pp. 134-150.

Shimizu,Y. and Itakura,T. (1991): Calculation of Flow and Bed Deformation with a General Non-Orthogonal Coordinate System, Proc. of XXIV IAHR Congress, Spain, C-2, pp.41-48.

Takebayashi, H. (2005): River Configuration in Middle-Lower Reach of River Basin, Journal of Japan Society of Fluid Mechanics, Vol. 24, pp. 27-36.

Takebayashi, H., Egashira, S. and Okabe, T. (2003): Braided streams formed on beds with non-uniform sediment, Proc. 3nd IAHR Symposium on River, Coastal and Estuarine Morphodynamics, pp.787-798.

Thorne, C.R., and Osman, A.M. (1988): Riverbank stability analysis II: Application, Journal of Hydraulic Engineering, Vol. 114, No. 2, pp. 151-172.